Published in final edited form as:
Cell. 2010 May 28; 141(5): 786–798. doi:10.1016/j.cell.2010.03.049.

Actin-Bundling Protein TRIOBP Forms Resilient Rootlets of Hair Cell Stereocilia That Are Essential for Hearing

Shin-ichiro Kitajiri[1,10], **Takeshi Sakamoto**[2], **Inna A. Belyantseva**[1], **Richard J. Goodyear**[3], **Ruben Stepanyan**[4], **Ikuko Fujiwara**[5], **Jonathan E. Bird**[1], **Saima Riazuddin**[1,11], **Sheikh Riazuddin**[6], **Zubair M. Ahmed**[1,11], **Jenny E. Hinshaw**[7], **James Sellers**[2], **James R. Bartles**[8], **John A. Hammer III**[5], **Guy P. Richardson**[3], **Andrew J. Griffith**[9], **Gregory I. Frolenkov**[4], and **Thomas B. Friedman**[1,*]

[1] Laboratory of Molecular Genetics, National Institute on Deafness and Other Communication Disorders, National Institutes of Health, Rockville, MD 20850, USA

[2] Laboratory of Molecular Physiology, National Heart, Lung and Blood Institute, National Institutes of Health, Bethesda, MD 20892, USA

[3] School of Life Sciences, University of Sussex, Falmer, Brighton BN1 9QG, UK

[4] Department of Physiology, University of Kentucky, Lexington, KY 40536, USA

[5] Laboratory of Cell Biology, National Heart, Lung and Blood Institute, National Institutes of Health, Bethesda, MD 20892, USA

[6] National Center of Excellence in Molecular Biology, University of the Punjab, Lahore 54700, Pakistan

[7] Structural Cell Biology Section, National Institute of Diabetes, and Digestive and Kidney Disease, National Institutes of Health, Bethesda, MD 20892, USA

[8] Department of Cell and Molecular Biology, Feinberg School of Medicine, Northwestern University, Chicago, IL 60611, USA

[9] Molecular Biology and Genetics Section, National Institute on Deafness and Other Communication Disorders, National Institutes of Health, Rockville, MD 20850, USA

SUMMARY

Inner ear hair cells detect sound through deflection of mechanosensory stereocilia. Each stereocilium is supported by a paracrystalline array of parallel actin filaments that are packed more densely at the

[*]Correspondence: Thomas B. Friedman, PhD. friedman@nidcd.nih.gov, Fax: 301-402-7580, friedman@nidcd.nih.gov.
[10]Present address: Department of Otolaryngology - Head and Neck Surgery, Kyoto University Graduate School of Medicine, Sakyo-ku, Kyoto 606-8507, Japan
[11]Present address: Divisions of Pediatric Otolaryngology Head & Neck Surgery and Ophthalmology, Children's Hospital Research Foundation, Cincinnati, OH 45215, USA

ACCESSION NUMBERS
Espin 3A GenBank AY587568
TRIOBP-4 GenBank DQ228002

SUPPLEMENTAL DATA
Supplemental Data include Supplemental Experimental Procedures five figures, one movie and can be found with this article online at http://www.cell.com/cgi/content/full/xxxxxxx

base, forming a rootlet extending into the cell body. The function of rootlets and the molecules responsible for their formation are unknown. We found that TRIOBP, a cytoskeleton-associated protein mutated in human hereditary deafness DFNB28, is localized to rootlets. *In vitro*, purified TRIOBP isoform 4 protein organizes actin filaments into uniquely dense bundles reminiscent of rootlets, but distinct from bundles formed by espin, an actin cross-linker in stereocilia. We generated mutant *Triobp* mice (*Triobp*$^{\Delta ex8/\Delta ex8}$) that are profoundly deaf. Stereocilia of *Triobp*$^{\Delta ex8/\Delta ex8}$ mice develop normally, but fail to form rootlets and are easier to deflect and damage. Thus, F-actin bundling by TRIOBP provides durability and rigidity for normal mechanosensitivity of stereocilia and may contribute to resilient cytoskeletal structures elsewhere.

INTRODUCTION

Hearing depends upon sound-induced deflections of mechanosensory stereocilia, actin-based microvilli-like projections on the apical surface of each cochlear hair cell organized into ranks of increasing height (Figure 1A). Nanometer-scale deflections tension the tip links between stereocilia and gate cation-selective mechanotransduction channels present on all but the tallest stereocilia (Beurg et al., 2009). The mechanical properties of each stereocilium must be precisely tuned for optimal sensitivity.

Mammalian stereocilia contain a core of uniformly-spaced polarized actin filaments inter-connected with espin and fimbrin/plastin (reviewed in Frolenkov et al., 2004). The barbed ends of the filaments are oriented toward the stereocilia tips, a site of actin monomer addition (Schneider et al., 2002). These filaments form a paracrystalline array that confers rigidity and allows each stereocilium to act as a stiff lever. When deflected, stereocilia pivot about their insertion points near the apical surface of the cell where the diameter of stereocilia tapers (Crawford et al., 1989; Karavitaki and Corey, 2006). Actin filament topology within the taper differs from the main stereocilia core. In this region, transmission electron microscopy (TEM) reveals a rootlet; an electron dense structure that penetrates into the cell body and also extends a comparable distance into the stereocilia core (Flock and Cheung, 1977) (Figure 1A). Similar rootlet structures were observed at the base of intestinal microvilli (Matsudaira and Burgess, 1982). Rootlets were proposed to anchor stereocilia into the actin-rich meshwork of the cuticular plate and/or provide flexible elements for durable pivoting of stereocilia about their tapers (Furness et al., 2008; Tilney et al., 1983; Tilney et al., 1986). However, in the absence of experimental models, the role of rootlets in hair bundle micromechanics and the molecules that guide their development remain elusive.

Here we show that TRIOBP is an actin-bundling protein that is critical for rootlet formation. Mutations of human *TRIOBP*, a gene encoding multiple isoforms, are associated with profound, prelingual deafness DFNB28 (MIM #609823) (Riazuddin et al., 2006; Shahin et al., 2006). The alternative splice isoforms of TRIOBP are produced through the use of two alternate promoters and can be grouped into three classes (Figure 1). The first are long transcripts that utilize a distal promoter upstream of exon 1 and terminate in exon 24, which encodes TRIOBP-5 (~218-kDa) in humans (Figure 1B). The second class is initiated from the same promoter but terminates immediately after exon 6, and encodes a shorter protein product, TRIOBP4 (~107-kDa) that contains the repeat motifs of exon 6 but none of the carboxy domains of TRIOBP-5. The third class, represented by TRIOBP-1 (~72-kDa; Seipel et al., 2001) is initiated from a promoter downstream of exon 6. TRIOBP-1 encodes a protein that does not contain the N-terminal internal repeat motifs, but does include the carboxy domains of TRIOBP-5 encoded by exons 11–24 (Figure 1B). Thus, TRIOBP-1 and TRIOBP-4 share no exons or amino acid coding sequence. Over-expression studies have suggested that TRIOBP-1 (previously named TARA) binds and stabilizes the actin cytoskeleton in HeLa cells (Seipel et al., 2001). While TRIOBP-1 is ubiquitous, TRIOBP-4 and TRIOBP-5 are expressed

predominantly in the eye and inner ear (Riazuddin et al., 2006; Shahin et al., 2006). To date, all of the mutations of *TRIOBP* causing human deafness DFNB28 are located in exon 6 (Figure 1B), and only affect TRIOBP-4 and TRIOBP-5 (TRIOBP-4/5).

All three isoform classes of TRIOBP localized to the stereocilia rootlets of inner ear hair cells. *In vitro*, purified TRIOBP-4 organizes actin filaments into bundles of unusually high density that resembled stereocilia rootlets. We engineered a TRIOBP-4/5 deficient mouse recapitulating human DFNB28 deafness. In this mouse, rootlets fail to develop resulting in stereocilia that were abnormally flexible at the pivot points and easily damaged by over-stimulation. Thus, the bundling of actin filaments by TRIOBP is essential for the biogenesis of rootlets that provide durable flexibility at the taper and mechanical rigidity to the stereocilia bundle.

RESULTS

TRIOBP Localizes to Stereocilia Rootlets

To determine the subcellular localization of the three different TRIOBP isoform classes, we developed and validated isoform-specific antibodies using TRIOBP-4/5 null mice described below (Figures 1D and S1). One antiserum detected only TRIOBP-5, while another detected both TRIOBP-1 and TRIOBP-5 (TRIOBP-1/5), and a third detected TRIOBP-4 and TRIOBP-5 (TRIOBP-4/5). All antisera labeled stereocilia rootlets of cochlear hair cells (Figures 2A–C, 2E–F, S1A, S1C, S1E and S1G-H). In addition, both TRIOBP-5 and TRIOBP-4/5 antisera labeled several types of non-sensory cells, in particular the actin-based processes of pillar and Deiters' cells (Figures 1A and 2D).

At P1–2, when stereocilia rootlets begin to develop, TRIOBP-5 staining was localized at the base of stereocilia (Figures S1A, S1C, S1E). However, by P14 TRIOBP-5 was predominantly observed along the segment of the mature rootlet that is within the cuticular plate (Figures 2A–C and S1G-H). In some instances, TRIOBP-5 labeling of the rootlet also extended into the taper region (Figures S1K-L), but little or no labeling was observed along the entire length of stereocilia (Figures 2B–C). By comparison, TRIOBP-4/5 antiserum labeled the entire length of a stereocilium in addition to distinct labeling of the rootlets (Figures 2E–F). Irrespective of the isoform-specific differences, both TRIOBP-4/5 and TRIOBP-5 antisera labeled the actin-rich stereocilia rootlets indicating their potential importance for rootlet function and/or formation.

TEM examination of post-embedded immunogold labeled thin sections confirmed that TRIOBP-5 was localized to the rootlets of P6 cochlear hair cells stereocilia, but not along the length of the stereocilia (Figure 2G). A non-specific IgG control did not show immunoreactivity within the cuticular plate or at the taper (data not shown). The distribution of gold particles in cross-sections of the rootlets (Figure 2H–J) indicated that TRIOBP may be associated predominantly with actin filaments at the rootlet periphery.

TRIOBP-4 Binds F-actin Filaments

High-speed actin co-sedimentation, which pellets all F-actin and F-actin- associated proteins, was performed to determine if *in vitro* purified TRIOBP-4 (136 kDa) has F-actin binding activity. A constant concentration of GFP-TRIOBP-4 (2 μM) was mixed with increasing amounts of F-actin followed by high-speed sedimentation (385,000 x g_{max} x 15 min). We found that GFP-TRIOBP-4 co-sediments with F-actin (Figure 3A). In the absence of F-actin, GFP-TRIOBP-4 did not sediment, showing that GFP-TRIOBP-4 did not form oligomers on its own (Figure 3A). The binding affinity K_d of GFP-TRIOBP-4 for F-actin was 0.94 ± 0.02 μM, as compared to 0.15 μM for espin (Bartles et al., 1998).

To establish where TRIOBP-4 might bind along F-actin, we incubated GFP-TRIOBP-4 together with TMR-labeled actin and observed filaments using total internal reflection fluorescence (TIRF) microscopy. We found that GFP-TRIOBP-4 was distributed along the length of actin filaments (Figure 3B). We also noted a significant increase in TMR-fluorescence of individual filamentous actin structures when formed in the presence of GFP-TRIOBP-4 as compared to controls where it was omitted. This suggested that in addition to binding, TRIOBP-4 may also have actin-bundling activity.

Purified TRIOBP-4 Packs Actin Filaments into Dense Bundles

To further investigate the putative bundling activity of TRIOBP-4, we used a low-speed co-sedimentation assay, which pellets only bundled actin filaments. GFP-TRIOBP-4 or F-actin alone did not sediment at 22,000 x g_{max} x 20 min. The level of GFP-TRIOBP-4 binding at saturation was quantified using a constant concentration of F-actin mixed with increasing amounts of GFP-TRIOBP-4 in a low-speed co-sedimentation assay. At saturation, one TRIOBP-4 molecule was bound per 3 to 4 actin subunits (TRIOBP-4/actin = 0.29 ± 0.01 mol/mol, Figure 3C). By comparison, one espin molecule was reported to bind approximately 4 actin subunits at saturation (Chen et al., 1999).

Under the same conditions as in the low speed co-sedimentation assay, actin filaments were formed on a monolayer lipid membrane, negatively stained, and imaged using TEM. In contrast to actin filaments formed without GFP-TRIOBP-4, addition of GFP-TRIOBP-4 promoted organization of actin filaments into prominent bundles (Figure 3D, lower). Image analyses revealed that the spatial periodicity of actin filaments bundled with GFP-TRIOBP-4 (Figure 4A) was 8.2±1.4 nm (mean±SD; n = 145), which coincides with an inter-filament distance of ~8 nm within stereocilia rootlets of guinea pig hair cells (Itoh, 1982). The distance between filaments bundled with a positive control, purified espin 3A (35kDa) (Figure 4B), was 11.9 ±2.1 nm (n = 148), which agrees well with 12.6±0.2 nm from small-angle X-ray scattering measurements (Purdy et al., 2007). Unlike with espin 3A, the 2D actin rafts formed in the presence of GFP-TRIOBP-4 always showed densely packed actin bundles with no visible inter-filament spacing or linkages (Figure 4A). When observing F-actin alone, we occasionally found patches of filaments that were aligned in parallel. In these cases, the distance between the centers of two adjacent filaments was 7.2±1.4 nm (n = 111; Figures 4C–4D), which resembles the ~7-nm diameter of F-actin. We conclude that GFP-TRIOBP-4 organizes F-actin into a highly ordered dense bundle where filaments are almost as close as they can be to one another. We repeated these experiments without a GFP fusion tag on TRIOBP-4 and made the same observations (data not shown).

In a pyrene-actin assembly assay, TRIOBP-4 (1.0 μM) without a GFP-tag (Figure 4E) or with GFP (Figure S2) had no noticeable effect on actin nucleation, but it partially inhibited actin polymerization. The inhibition of actin assembly by TRIOBP-4 may result from decreased barbed end availability and/or actin monomer sequestration as reported for espin-3A and -3B (Sekerkova et al., 2004). We next used TIRF microscopy to visualize actin bundle formation by GFP-TRIOBP-4 in real time. In the presence of GFP-TRIOBP-4, elongating actin filaments readily fused to one another when coming into close apposition (Figure 5 and Movie S1). F-actin structures coalesced or zipped together to form thicker bundles (Figures 5A and 5B), whereas in the absence of TRIOBP-4, actin filaments grew but hardly ever fused to each other (Movie S1). In addition to fusion, some bundles elongated from both ends at approximately the same rate, suggesting that actin bundles formed *in vitro* by TRIOBP-4 can consist of anti-parallel filaments (Figure 5C). We conclude that *in vitro*, TRIOBP-4 is sufficient to organize F-actin into dense bundles that have properties resembling hair cell rootlets observed *in vivo*.

Triobp$^{\Delta ex8/\Delta ex8}$ Mice Are Deaf

To determine if TRIOBP-4 and/or TRIOBP-5 are necessary for rootlet formation, we engineered a mutant mouse (*Triobp*$^{\Delta ex8}$), in which *Triobp* exon 8 (orthologous to human exon 6, Figure 1B), was replaced with a lacZ reporter casette (Figure S3A). In *Triobp*$^{\Delta ex8/+}$ mice, β-galactosidase was detected along the entire length of the sensory epithelium of the organ of Corti, in the sensory maculae of the vestibular end-organs and in a subpopulation of the spiral ganglion neurons (Figure S4A). Particularly strong X-gal staining was observed in the inner (IHCs) and outer hair cells (OHCs) and their adjacent supporting cells (Figure S4B) corresponding with TRIOBP-4/5 immunolocalization (Figure 2). In cross-sections of P35 *Triobp*$^{\Delta ex8/\Delta ex8}$ cochleae, no gross morphological abnormalities were observed (Figures S4D-E).

We next determined the thresholds of auditory-evoked brainstem responses (ABR) in *Triobp*$^{\Delta ex8/\Delta ex8}$, *Triobp*$^{\Delta ex8/+}$, and *Triobp*$^{+/+}$ adult littermates. Normal ABR thresholds and waveforms were observed in wild type and heterozygous mice. However, *Triobp*$^{\Delta ex8/\Delta ex8}$ mice did not respond to either a 100 dB sound pressure level (SPL) click or tone bursts at 8 kHz to 32 kHz, indicating that they are profoundly deaf (Figure S4C), recapitulating human DFNB28 deafness.

As expected, the expression of TRIOBP-5 mRNA (Figure S3C) and TRIOBP-4/5 protein (Figures S1B and S1D) in the inner ear of *Triobp*$^{\Delta ex8/\Delta ex8}$ mice was ablated, whilst TRIOBP-1 isoform was retained (Figures S1F and S3C). To determine the phenotype of mice deficient for TRIOBP-1, two different knockout alleles were generated that simultaneously truncated TRIOBP-1 and TRIOBP-5. Both alleles resulted in embryonic lethality (data not shown). Thus, TRIOBP-4 and/or TRIOBP-5 are essential for hearing whilst ubiquitously expressed TRIOBP-1 has an additional, essential role during development. If TRIOBP-1 is also essential for human development, it might explain why all mutations causing human deafness DFNB28 are clustered upstream of the alternative promoter for the transcript encoding TRIOBP-1 (Figure 1B).

Stereocilia Rootlets Fail to Develop in *Triobp*$^{\Delta ex8/\Delta ex8}$ Mice

Since TRIOBP-4/5 isoforms were immunolocalized to rootlets, we examined rootlet ultrastructure in wild type and *Triobp*$^{\Delta ex8/\Delta ex8}$ hair cells with TEM. At P1, no obvious rootlet structures were observed in both wild type and *Triobp*$^{\Delta ex8/\Delta ex8}$ hair cells, although filaments appear to extend a short distance from the tapered base of the stereocilia into the cuticular plate (Figures 6A and 6B). Between P1 and P16 in wild type hair cells, a dense rootlet structure progressively formed at the base of stereocilia penetrating into the cuticular plate and taper region (Figure 6A). In *Triobp*$^{\Delta ex8/\Delta ex8}$ mice, rootlets did not form (Figure 6B). Even by P16, rootlets were not observed in mutant hair cells (Figure 6B), indicating that formation of these structures was disrupted in *Triobp*$^{\Delta ex8/\Delta ex8}$ mice rather than developmentally delayed. Although TRIOBP-1 is expressed in *Triobp*$^{\Delta ex8/\Delta ex8}$ mice, and is concentrated at the base of stereocilia (Figure S1F), it cannot compensate for the loss of TRIOBP-4/5 function in rootlet formation. Similarly, espin (Zheng et al., 2000), an essential actin bundling protein found along the length of the stereocilia in both wild type and *Triobp*$^{\Delta ex8/\Delta ex8}$ mice, failed to compensate for the absence of TRIOBP-4/5 (Figure S4F, left panels). We conclude that TRIOBP-4 and/or TRIOBP-5 are necessary to form mature stereocilia rootlets.

In the wild type, rootlet length is proportional to the height of its conjugate stereocilium. Therefore, it was suggested that growth of these two structures is regulated by a common process (Furness et al., 2008). However, even in the absence of rootlets, the length of *Triobp*$^{\Delta ex8/\Delta ex8}$ stereocilia was not grossly affected (Figures 6B, 6D and S1). Conversely, in deaf whirler mice, which have abnormally short stereocilia (Belyantseva et al., 2005; Mburu

et al., 2003), rootlet lengths within the cuticular plate also appears to be unaltered (Figures S1J–S1L). Therefore, the lengths of mature rootlets and stereocilia seem to be controlled independently.

Triobp$^{\Delta ex8/\Delta ex8}$ Stereocilia Progressively Degenerate

When observed using scanning electron microscopy (SEM), stereocilia bundles of P7 *Triobp*$^{\Delta ex8/\Delta ex8}$ cochlear hair cells were almost indistinguishable from wild type. By P16 however, widespread fusion and degeneration of stereocilia was evident throughout *Triobp*$^{\Delta ex8/\Delta ex8}$ cochleae (Figures 6C and 6D). Degeneration occurred during a critical time when hearing thresholds are normally being established; this alone could explain the profound deafness of *Triobp*$^{\Delta ex8/\Delta ex8}$ mice exhibited at P16. We also observed subtle, yet consistent defects in stereocilia bundles of *Triobp*$^{\Delta ex8/\Delta ex8}$ hair cells as early as P1. In both IHCs and OHCs, peripheral stereocilia often deviated outward away from their normal position (arrows, Figure S4F, top images). This phenomenon was never observed in heterozygous normal hearing littermates (Figure S4F, bottom images). In the wild type, TRIOBP-5 is present at the base of stereocilia prior to rootlet formation as early as E16.5 (data not shown) through P1–2 (Figures S1A–S1C). Therefore, TRIOBP-4/5 may help anchor or confine each stereocilium to a specific position in the cuticular plate even at P0 before an obvious rootlet structure has formed.

Triobp$^{\Delta ex8/\Delta ex8}$ Hair Cells Have Normal Mechano-Electrical Transduction

Since TRIOBP-4 is localized along the length of stereocilia, we considered the possibility that mechano-electrical transduction (MET) could be affected in *Triobp*$^{\Delta ex8/\Delta ex8}$ hair cells. We examined MET responses evoked by deflections of hair bundles using a rigid piezo-driven glass probe (Figure 7A) in live cochlear hair cells of P4–P9 *Triobp*$^{\Delta ex8/\Delta ex8}$ and *Triobp*$^{\Delta ex8/+}$ littermates. The absence of TRIOBP-4/5 did not affect MET responses in OHCs (Figure 7B) and IHCs (data not shown). The maximum MET current was similar in *Triobp*$^{\Delta ex8/+}$ and *Triobp*$^{\Delta ex8/\Delta ex8}$ OHCs (*Triobp*$^{\Delta ex8/+}$: 0.68±0.06 nA, n=4; *Triobp*$^{\Delta ex8/\Delta ex8}$: 0.65±0.02 nA, n=3; p=0.66), and the MET current-displacement relationships were almost identical (Figure 7C). Time constants of fast (τ_{fast}) and slow (τ_{slow}) adaptation were also similar (*Triobp*$^{\Delta ex8/+}$: τ_{fast}=210±30 μs, τ_{slow}=2.8±0.3 ms, n=4; *Triobp*$^{\Delta ex8/\Delta ex8}$: τ_{fast}=260±50 μs, τ_{slow}=3.2±1.1 ms, n=3; double exponential fit of the responses). Thus, the absence of rootlets and TRIOBP-4/5 do not interfere with delivery, assembly or function of the MET machinery prior to the onset of hearing.

Rootlets Provide Rigidity to Stereocilia

Experiments showing normal MET responses in *Triobp*$^{\Delta ex8/\Delta ex8}$ hair cells did not provide insight into potential changes of stereocilia stiffness, because the rigid piezo-driven probe deflected the hair bundle to a pre-determined angle independent of its stiffness. Consequently, we deflected stereocilia bundles of live IHCs using calibrated fluid-jet stimuli (Figure 7D; for fluid-jet calibration see Figure S5). We found that *Triobp*$^{\Delta ex8/\Delta ex8}$ stereocilia are about twice more flexible as compared to *Triobp*$^{\Delta ex8/+}$ stereocilia, when deflected by fluid-jet stimuli of progressively increasing intensity. This difference was approximately 4-fold when deflected using progressively decreasing stimuli (Figure 7E, left). These changes in stereocilia bundle flexibility may be due to either less rigid pivot points and/or more flexible stereocilia cores. However, we did not observe significant bending of stereocilia in *Triobp*$^{\Delta ex8/\Delta ex8}$ hair cells by TEM or SEM (Figure 6), suggesting that the increased flexibility observed in *Triobp*$^{\Delta ex8/\Delta ex8}$ hair cells was likely due to changes in the mechanical properties at the stereocilia taper.

The dependence of stereocilia bundle stiffness upon the order of stimulus presentation in *Triobp*$^{\Delta ex8/\Delta ex8}$ mice also suggests that the stereocilia of mutant mice are more fragile. Indeed,

after *Triobp*$^{\Delta ex8/\Delta ex8}$ stereocilia were deflected once by a relatively large stimulus, their pivot stiffness often decreased (Figure 7E, left; note a prominent non-linearity at negative stimuli larger than 10 mm Hg). Pivotal stiffness of *Triobp*$^{\Delta ex8/+}$ stereocilia did not depend on the order of stimuli presentation indicating that stereocilia with rootlets are likely to withstand larger stimuli without suffering irreversible damage. It should be noted, however, that stereocilia of *Triobp*$^{\Delta ex8/\Delta ex8}$ mice are less stiff even before applying large deflections. The difference between stiffness of *Triobp*$^{\Delta ex8/\Delta ex8}$ and *Triobp*$^{\Delta ex8/+}$ hair bundles was statistically significant even for small (±6 mm Hg) stimuli presented with increasing intensities (Fig. 7F). These data indicate that rootlets not only make stereocilia more resistant to deflection-induced damage, but also provide essential stiffness to the hair bundle.

Besides rootlets, a variety of extracellular filaments interconnecting stereocilia could contribute to mechanical stiffness of the stereocilia bundle in mammalian hair cells (Beurg et al., 2008). To test the relative contributions of rootlets alone, we ablated the filamentous links that interconnect stereocilia. In young postnatal IHCs, exposure of the bundle to extracellular Ca^{2+}-free medium supplemented with BAPTA eliminated tip links and most immature side-links (Figures 7G–7H). After BAPTA treatment (Figure 7E, right), we observed even larger differences between the pivotal stiffness of *Triobp*$^{\Delta ex8/\Delta ex8}$ and *Triobp*$^{\Delta ex8/+}$ stereocilia. There was about a three-fold difference when stimuli were presented at increasing intensities, and almost a ten-fold difference when the bundle first underwent a large deflection.

In phenotypically wild type *Triobp*$^{\Delta ex8/+}$ IHCs analyzed before and after treatment, BAPTA produced only a slight decrease in pivotal stiffness by 14%±9% (Figure 7F). In contrast, TRIOBP-4/5 deficiency resulted in a substantial drop in stiffness of mutant *Triobp*$^{\Delta ex8/\Delta ex8}$ stereocilia bundles by 43%±8% in the presence of tip links, and even a further drop (overall, by 64%±6%) in *Triobp*$^{\Delta ex8/\Delta ex8}$ bundles treated with BAPTA (Figure 7F). Thus, at least in young postnatal IHCs, stereocilia rootlets are a major contributor to hair bundle stiffness because elimination of rootlets has a more profound effect on the stiffness compared to ablation of stereocilia links (Figure 7F). Taken together, our data suggests that even though the MET machinery is operational in *Triobp*$^{\Delta ex8/\Delta ex8}$ hair cells, these cells are unlikely to have normal mechanosensitivity *in vivo* due to both the decreased pivotal stiffness and increased fragility of the stereocilia bundle.

DISCUSSION

Our results demonstrate that TRIOBP, an actin-associated protein mutated in human deafness DFNB28, is able to bundle parallel F-actin into unusually dense structures with no obvious spacing between filaments. A further principal finding is the importance of TRIOBP in the formation of stereocilia rootlets, which are essential for hearing because they determine stiffness and durability of the hair bundle, a mechanosensory organelle on the apical surface of a hair cell.

TRIOBP-4 Bundles Actin Filaments

In vitro, TRIOBP-4 alone was sufficient to organize actin filaments into dense bundles that resembled stereocilia rootlets *in vivo*. Inter-filament spacing in bundles formed by TRIOBP-4 is significantly smaller than in bundles formed by espin 3A. In contrast to espin 3A, TRIOBP-4 might not be intercalated between actin filaments. Instead, two observations indicate that TRIOBP-4 and/or TRIOBP-5 may wrap externally around actin filaments. First, immuno-EM suggests that TRIOBP is located at the periphery of stereocilia rootlets. Second, the reduced inter-filament spacing in TRIOBP-4 bundles may leave insufficient space for a globular cross-linker (Figure 4), although we cannot exclude the possibility that TRIOBP-4 might take on an extended conformation along the filament.

How do Stereocilia Rootlets Form?

Several hypotheses are plausible. Actin filaments of the rootlets may form *de novo* within the cuticular plate and subsequently coalesce into bundles. However, this leaves unexplained how a rootlet becomes precisely aligned below its cognate stereocilium. An alternative explanation comes from studies of thin filaments of striated muscle where the major sites of actin monomer addition are at the pointed ends (Littlefield et al., 2001). The pointed ends of actin filaments are located towards the base of the stereocilia core. Perhaps as the stereocilia core develops and reaches its mature diameter and length, monomer addition occurs at the pointed ends and extends actin filaments into the cell body (Tilney and DeRosier, 1986). Subsequently, actin filaments may become bundled by TRIOBP and integrated with filaments of the cuticular plate. How exactly rootlet growth is regulated is unknown, but it apparently requires TRIOBP-4 and/or TRIOBP-5.

Why does the loss of rootlets cause stereocilia degeneration?

Stereocilia without rootlets are more fragile and flexible at the pivot point (Figure 7). Their actin cores may therefore be readily damaged, which is known to result in stereocilia disassembly (Belyantseva et al., 2009). The increased flexibility may also contribute to the fusion of *Triobp*$^{\Delta ex8/\Delta ex8}$ stereocilia plasma membranes that is observed in late postnatal development (Figure 6D). Alternatively, rootlets may act as molecular gatekeepers or filters allowing selected proteins to enter the stereocilia. Indeed, while myosins 1c, 7a and 15a do enter and move along actin filaments in stereocilia (Belyantseva et al., 2005), exogenous myosin 10 does not (data not shown). The basis of this selectivity is unknown, but insight can be taken from reports that myosin 10 processivity on actin is sensitive to inter-filament spacing (Nagy et al., 2008). The dense configuration of actin filaments in a rootlet may provide a selective substrate for a subset of myosins and associated cargos that are important for stereocilia maintenance.

Rootlets Provide Durability and Pivotal Stiffness of Stereocilia

In mice, rootlets develop in the early stages of postnatal development (Figure 6B). While they are forming, a variety of transient extracellular filamentous links between stereocilia may facilitate upright posture of hair bundles (Goodyear et al., 2005). When rootlets are eventually formed and provide a durable, rigid structural element, transient stereocilia links may no longer be needed to maintain hair bundle architecture, and disappear.

During deflection of the hair bundle, the cross-bridged actin filaments within stereocilia were proposed to slide short distances relative to each other so that the cross-bridges become tilted relative to the long axis of an actin bundle (Tilney et al., 1983). Excessive sliding was thought to damage these cross-bridges. A characteristic feature of the rootlet is a denser packing of actin filaments compared to that of actin core of stereocilia. This smaller inter-filament distance may result in less sliding of actin filaments and therefore in a decrease of stimulation-induced damage to a stereocilium. In addition, F-actin bundled by TRIOBP at the periphery of a bundle may not have internal cross-bridges between filaments, allowing them to more easily slide past one another providing durable flexibility at the taper.

In summary, we have demonstrated that TRIOBP-4/5 is an actin-bundling protein essential for rootlet formation and establishing necessary durability and pivotal stiffness of stereocilia. The stiffness of a stereocilium at the pivot point is thought to act in conjunction with the elusive “gating spring” that opens the transduction channel. Adjustment of pivotal stiffness with TRIOBP-4/5 may therefore represent a critical step in achieving optimal micromechanical sensitivity of a hair cell. Finally, since TRIOBP-4 and -5 are expressed in other tissues beyond the inner ear, and TRIOBP-1 is essential for viability of the embryo, we infer that future studies will reveal TRIOBP as an unique F-actin organizer in diverse cell types.

EXPERIMENTAL PROCEDURES

Detailed methods can also be found in the Extended Experimental Procedures available online.

Triobp-4/5 Mutant Mice

Exon 8 of *Triobp* (Figure S1A) was deleted by using a general strategy (Ikeya et al., 2005) and nBLUEneo and DT-A(B.DEST) vectors provided by Makoto Ikeya. The 5' arm (8 kb) and 3' arm (4 kb) of the targeting vector were obtained from clone RP23-414K1 (BACPAC Resources Center, CA). Except for the first 5 bp, all of *Triobp* exon 8 (2,288 bp) was removed and a nLacZ reporter cassette inserted in frame with the upstream protein sequence of *Triobp*. Bruce4 ES cells were electroporated with *Not*I-linearized targeting vector, and 1,056 ES clones were screened for homologous recombination events. PCR-positive ES cell clones were evaluated by Southern blot analyses using specific probes (Figure S1A). Two independent ES cell clones produced chimeric mice. Heterozygotes for the targeted allele were obtained from both lines. Mice with an engineered deletion of exon 8 is designated *C57BL/6-Triobp*^{tm1Tbf} while *Triobp*$^{\Delta ex8/\Delta ex8}$ is used as a short symbol. Germline transmission of this mutation was confirmed by Southern blot (Figure S1B). The neo cassette was removed by mating with C57BL/6-Tg(Zp3-cre)93Knw/J mice and heterozygotes were outbred for eight generations to C57BL/6J. *Triobp*$^{\Delta ex8/\Delta ex8}$ mice from the two independent lines have identical mutant phenotypes.

Purification of Actin, GFP-TRIOBP-4, and Espin 3A

Actin was purified from rabbit skeletal muscle as described (Spudich and Watt, 1971). To separate actin monomers and oligomers, a S-300 gel filtration column was used. Monomeric actin was stored in G-buffer (0.2 mM ATP, 1 mM NaN_3, 0.1 mM $CaCl_2$, 0.5 mM DTT, and 2 mM Tris-HCl, pH 8.0). Actin in KMEI buffer (50 mM KCl, 1 mM $MgCl_2$, 1 mM EGTA, 10 mM imidazole, pH 7.0) was labeled with tetramethylrhodamine-5-maleimide (TMR, Invitrogen) and purified by centrifugation, dialysis and gel filtration as described (Fujiwara et al., 2002). The concentrations of actin and TMR were estimated using the extinction coefficients A_{290} = 26,600/M/cm and A_{550} = 96,900/M/cm, respectively. The concentration of labeled actin was determined by subtracting 0.208 times the A_{550} value from the A_{290} value.

Triobp-4 cDNA (GenBank DQ228002) encoding an ~107 kDa protein was inserted into pFastBac 1 (Invitrogen). cDNA encoding green fluorescent protein (GFP) was sub-cloned into the N-terminus of the *Triobp-4* cDNA and a FLAG epitope tag (DYKDDDDK; GACTACAAGGACGACGATGATAAG) followed by a translation stop codon (TAG) was added at the C-terminus. Bacmids were generated, and used to express GFP-TRIOBP-4-FLAG in Sf9 insect cells. GFP-TRIOBP-4-FLAG protein was affinity purified from cell lysates using anti-FLAG resin (Sigma). Purified GFP-TRIOBP-4-FLAG protein was further purified by gel filtration (AKTA FPLC, Superose 12 10/300GL, Amersham Biosciences). The concentration of GFP-TRIOBP-4-FLAG in buffer (10 mM MOPS pH 7.4, 100 mM KCl, 0.1 mM EGTA, and 2 mM $MgCl_2$) was determined by measuring the absorbance in solution using the extinction coefficient of 80810 $M^{-1}cm^{-1}$. TRIOBP-4-FLAG protein without GFP was also expressed and purified by the same procedure described above. Espin 3A (AY587568; Sekerkova et al., 2004) with an N-terminal 6xHis tag was purified as described (Chen et al., 1999) and stored in 0.1 M KCl, 1 mM DTT and 3 mM NaN_3, 10 mM Hepes-KOH, pH 7.4. The purity of each preparation of espin 3A and TRIOBP-4 was evaluated by SDS-PAGE.

2-D Rafts of F-actin

Two dimensional (2-D) rafts of actin filaments were formed using a modification of a technique (Taylor and Taylor, 1994; Volkmann et al., 2001) developed for decorating actin filaments with a myosin S1 fragment (Moore et al., 1970). Briefly, a 3:7 w/w lipid solution (total 1mg/

ml) of 1,2-dilaurylphosphatidylcholine (DLPT, Avanti Polar Lipids, Inc.) and didodecyldimethylammonium bromide (DDDMA, Fluka) in chloroform was spread on the surface of the polymerization buffer that contained 20 mM Na_2HPO_4, 50 mM KCl, 1 mM ATP, 2 mM $MgCl_2$, 1 mM EGTA, 1 mM DTT in a 20 μl Teflon well and incubated for 1 hr at 4°C. G-actin was added to a solution of purified GFP-TRIOBP-4-FLAG or purified espin 3A, or to a solution without an actin cross linker. Using a glass pipette this G-actin solution was mixed and injected into the polymerization buffer in a Teflon well and incubated for 14–16 hr at 4° C. 2D-actin paracrystalline arrays formed underneath the monolayer lipid membrane (Langmuir-Blodgett film). The film was transferred to 400-mesh carbon-coated copper grids, washed with polymerization buffer, negatively stained with 2% aqueous uranyl acetate. TEM images were taken at 100 keV with 35,000 magnification and 0.5 μm defocus (Philips CM120, Digital Micrograph). To measure the distance between actin filaments in the bundles, image analyses were performed as described (Volkmann et al., 2001). Briefly, images were processed using a fast Fourier transform (FFT) filter to detect spatial periodicity (Metamorph, Molecular Devices). Line scan intensity was measured across the filtered image of the bundles and then fit to a sum of Gaussian distributions using the maximal likelihood method. The distance between the peaks of these distributions represents the distance between the centers of adjacent actin filaments.

Actin Polymerization and TIRF microscopy

A solution-based pyrene-actin polymerization assay (Pollard 1983; Fujiwara et al., 2009) was used to examine the effect of purified recombinant GFP-TRIOBP-4. For TIRF assays, a flow cell (~7 μl) was made from #1 cover glasses (Kuhn and Pollard, 2005). Streptavidin (1mg/ml, Fluka, #85878) was loaded into the flow cell and excess washed out with 30 μl KMEI buffer. 15 μl of 20% TMR-labeled actin with or without GFP-TRIOBP-4 in polymerization buffer (50 mM KCl, 1 mM $MgCl_2$, 1 mM EGTA, 10 mM imidazole, pH 7.0, 100 mM DTT, 0.2 mM ATP, 15 mM glucose, 0.5% (w/v) methylcellulose, 40 μg/ml catalase and 200 ug/ml glucose oxidase) was applied to the flow cell. Actin filaments were observed at room temperature with a TIRF microscope (Olympus IX-71, PlanApo x100 oil 1.45 NA lens) and imaged with a cooled CCD camera (Spot 20.0, Diagnostic Instruments, Inc). The average fluorescence intensity was estimated using a line-scan along actin filaments with a 6 x 6 pixels region of interest (ImageJ, http://rsb.info.nih.gov/ij/).

Hair Cell Mechanotransduction and Deflection of Stereocilia

Organ of Corti explants in L-15 cell medium (Invitrogen) were observed at room temperature (TE2000, Nikon) using a 100x oil-immersion objective (1.3NA 0.2WD) and DIC. To access OHCs and IHCs, outermost cells were removed by gentle suction with a ~10 μm micropipette. Patch-clamp pipettes were filled with (mM): CsCl (140), $MgCl_2$ (2.5), Na_2ATP (2.5), EGTA (1.0), HEPES (5), osmolarity 325 mOsm, pH=7.35. The pipette resistance was 2–4 MΩ and series resistance was compensated (up to 80% at a 16 kHz bandwidth). For mechanotransduction recordings, hair bundles were deflected by a rigid glass probe driven by a piezoelectric actuator (PA 4/12, Piezosystem Jena) as described previously (Stepanyan & Frolenkov, 2009). For stereocilia deflection with a fluid-jet, pressure was generated using a High Speed Pressure Clamp (HSPC-1, ALA Scientific) and applied to the back of an 8–10 μm pipette filled with bath solution. The pipette tip was positioned at a distance of 9.5–11 μm in front of the hair bundle. It was determined that the force generated by this microjet depends linearly on the applied pressure with a slope of 0.13–0.21 nN/μm (Figure S5). The same pipette was used to deflect stereocilia bundles of *Triobp*$^{\Delta ex8/\Delta ex8}$ and *Triobp*$^{\Delta ex8/+}$ littermates. The steady-state pressure was adjusted to zero by monitoring debris movement in front of a fluid-jet. Movement of stereocilia was recorded for subsequent frame-by-frame computation of displacements using algorithms developed for quantifying electromotility of isolated OHCs (Frolenkov et al., 1997).

Supplementary Material

Refer to Web version on PubMed Central for supplementary material.

Acknowledgments

The authors thank M. Ikeya for advice and vectors, M. Streuli for mononclonal antiserum to TRIOBP-1/5, P. Belyantsev for drawings, and N. Gavara, M. Barzik, R. Chadwick, J. Schultz, and D. Drayna for discussions. This work was supported by NIDCD/NIH R01DC008861 and R01DC009434 to G.I.F., R01 DC004314 to J.R.B, the Wellcome Trust grant 071394/Z/03/Z to G.P.R, the HEC and MoST, Islamabad to S.R., and intramurals programs of NHLBI and NIDCD Z01 DK060100 to J.H., Z01 HL004232-08 to J.S., Z01 DC 000064 A.J.G and Z01 DC000048 to T.B.F.

References

Bartles JR, Zheng L, Li A, Wierda A, Chen B. Small espin: a third actin-bundling protein and potential forked protein ortholog in brush border microvilli. J Cell Biol 1998;143:107–119. [PubMed: 9763424]

Belyantseva IA, Boger ET, Naz S, Frolenkov GI, Sellers JR, Ahmed ZM, Griffith AJ, Friedman TB. Myosin-XVa is required for tip localization of whirlin and differential elongation of hair-cell stereocilia. Nat Cell Biol 2005;7:148–156. [PubMed: 15654330]

Belyantseva IA, Perrin BJ, Sonnemann KJ, Zhu M, Stepanyan R, McGee J, Frolenkov GI, Walsh EJ, Friderici KH, Friedman TB, et al. Gamma-actin is required for cytoskeletal maintenance but not development. Proc Natl Acad Sci USA 2009;106:9703–9708. [PubMed: 19497859]

Beurg M, Nam JH, Crawford A, Fettiplace R. The actions of calcium on hair bundle mechanics in mammalian cochlear hair cells. Biophys J 2008;94:2639–2653. [PubMed: 18178649]

Beurg M, Fettiplace R, Nam JH, Ricci AJ. Localization of inner hair cell mechanotransducer channels using high-speed calcium imaging. Nat Neurosci 2009;12:553–558. [PubMed: 19330002]

Chen B, Li A, Wang D, Wang M, Zheng L, Bartles JR. Espin contains an additional actin-binding site in its N terminus and is a major actin-bundling protein of the Sertoli cell-spermatid ectoplasmic specialization junctional plaque. Mol Biol Cell 1999;10:4327–4339. [PubMed: 10588661]

Crawford AC, Evans MG, Fettiplace R. Activation and adaptation of transducer currents in turtle hair cells. J Physiol 1989;419:405–434. [PubMed: 2621635]

Flock A, Cheung HC. Actin filaments in sensory hairs of inner ear receptor cells. J Cell Biol 1977;75:339–343. [PubMed: 318131]

Frolenkov GI, Belyantseva IA, Friedman TB, Griffith AJ. Genetic insights into the morphogenesis of inner ear hair cells. Nat Rev Genet 2004;5:489–498. [PubMed: 15211351]

Frolenkov GI, Kalinec F, Tavartkiladze GA, Kachar B. Cochlear outer hair cell bending in an external electric field. Biophys J 1997;73:1665–1672. [PubMed: 9284333]

Fujiwara I, Takahashi S, Tadakuma H, Funatsu T, Ishiwata S. Microscopic analysis of polymerization dynamics with individual actin filaments. Nat Cell Biol 2002;4:666–673. [PubMed: 12198494]

Fujiwara I, Remmert K, Hammer JA III. Direct observation of the uncapping of capping protein-capped actin filaments by CARMIL homology domain 3 (CAH3). J Biol Chem 2010;285:2707–2720. [PubMed: 19926785]

Furness DN, Mahendrasingam S, Ohashi M, Fettiplace R, Hackney CM. The dimensions and composition of stereociliary rootlets in mammalian cochlear hair cells: comparison between high- and low-frequency cells and evidence for a connection to the lateral membrane. J Neurosci 2008;28:6342–6353. [PubMed: 18562604]

Goodyear RJ, Marcotti W, Kros CJ, Richardson GP. Development and properties of stereociliary link types in hair cells of the mouse cochlea. J Compar Neurol 2005;485:75–85.

Ikeya M, Kawada M, Nakazawa Y, Sakuragi M, Sasai N, Ueno M, Kiyonari H, Nakao K, Sasai Y. Gene disruption/knock-in analysis of mONT3: vector construction by employing both in vivo and in vitro recombinations. Int J Dev Biol 2005;49:807–823. [PubMed: 16172977]

Itoh M. Preservation and visualization of actin-containing filaments in the apical zone of cochlear sensory cells. Hear Res 1982;6:277–289. [PubMed: 6806231]

Karavitaki, KD.; Corey, DP. Hair bundle mechanics at high frequencies: A test of series or parallel transduction. In: Nutall, AL., editor. Auditory Mechanisms: Processes and Models. Singapore: World Scientific; 2006. p. 286-292.

Kuhn JR, Pollard TD. Real-time measurements of actin filament polymerization by total internal reflection fluorescence microscopy. Biophys J 2005;88:1387–1402. [PubMed: 15556992]

Littlefield R, Almenar-Queralt A, Fowler VM. Actin dynamics at pointed ends regulates thin filament length in striated muscle. Nat Cell Biol 2001;3:544–551. [PubMed: 11389438]

Matsudaira PT, Burgess DR. Structure and function of the brush-border cytoskeleton. Cold Spring Harb Symp Quant Biol 1982;46:845–854. [PubMed: 6955108]

Mburu P, Mustapha M, Varela A, Weil D, El-Amraoui A, Holme RH, Rump A, Hardisty RE, Blanchard S, Coimbra RS, et al. Defects in whirlin, a PDZ domain molecule involved in stereocilia elongation, cause deafness in the whirler mouse and families with DFNB31. Nat Genet 2003;34:421–428. [PubMed: 12833159]

Moore PB, Huxley HE, DeRosier DJ. Three-dimensional reconstruction of F-actin, thin filaments and decorated thin filaments. J Mol Biol 1970;50:279–295. [PubMed: 5476917]

Nagy S, Ricca BL, Norstrom MF, Courson DS, Brawley CM, Smithback PA, Rock RS. A myosin motor that selects bundled actin for motility. Proc Natl Acad Sci USA 2008;105:9616–9620. [PubMed: 18599451]

Pollard TD. Measurement of rate constants for actin filament elongation in solution. Anal Biochem 1983;134:406–412. [PubMed: 6650826]

Purdy KR, Bartles JR, Wong GC. Structural polymorphism of the actin-espin system: a prototypical system of filaments and linkers in stereocilia. Phys Rev Lett 2007;98:058105. [PubMed: 17358907]

Riazuddin S, Khan SN, Ahmed ZM, Ghosh M, Caution K, Nazli S, Kabra M, Zafar AU, Chen K, Naz S, et al. Mutations in TRIOBP, which encodes a putative cytoskeletal-organizing protein, are associated with nonsyndromic recessive deafness. Am J Hum Genet 2006;78:137–143. [PubMed: 16385457]

Schneider ME, Belyantseva IA, Azevedo RB, Kachar B. Rapid renewal of auditory hair bundles. Nature 2002;418:837–838. [PubMed: 12192399]

Seipel K, O'Brien SP, Iannotti E, Medley QG, Streuli M. Tara, a novel F-actin binding protein, associates with the Trio guanine nucleotide exchange factor and regulates actin cytoskeletal organization. J Cell Sci 2001;114:389–399. [PubMed: 11148140]

Sekerkova G, Zheng L, Loomis PA, Changyaleket B, Whitlon DS, Mugnaini E, Bartles JR. Espins are multifunctional actin cytoskeletal regulatory proteins in the microvilli of chemosensory and mechanosensory cells. J Neurosci 2004;24:5445–5456. [PubMed: 15190118]

Shahin H, Walsh T, Sobe T, Abu Sa'ed J, Abu Rayan A, Lynch ED, Lee MK, Avraham KB, King MC, Kanaan M. Mutations in a novel isoform of TRIOBP that encodes a filamentous-actin binding protein are responsible for DFNB28 recessive nonsyndromic hearing loss. Am J Hum Genet 2006;78:144–152. [PubMed: 16385458]

Spudich JA, Watt S. The regulation of rabbit skeletal muscle contraction. I. Biochemical studies of the interaction of the tropomyosin-troponin complex with actin and the proteolytic fragments of myosin. J Biol Chem 1971;246:4866–4871. [PubMed: 4254541]

Stepanyan R, Frolenkov GI. Fast adaptation and Ca2+ sensitivity of the mechanotransducer require myosin-XVa in inner but not outer cochlear hair cells. J Neurosci 2009;29:4023–4034. [PubMed: 19339598]

Taylor KA, Taylor DW. Formation of two-dimensional complexes of F-actin and crosslinking proteins on lipid monolayers: demonstration of unipolar alpha-actinin-F-actin crosslinking. Biophys J 1994;67:1976–1983. [PubMed: 7858134]

Tilney LG, Egelman EH, DeRosier DJ, Saunder JC. Actin filaments, stereocilia, and hair cells of the bird cochlea. II. Packing of actin filaments in the stereocilia and in the cuticular plate and what happens to the organization when the stereocilia are bent. J Cell Biol 1983;96:822–834. [PubMed: 6682111]

Tilney LG, DeRosier DJ. Actin filaments, stereocilia, and hair cells of the bird cochlea. IV. How the actin filaments become organized in developing stereocilia and in the cuticular. plate Dev Biol 1986;116:119–129.

Volkmann N, DeRosier D, Matsudaira P, Hanein D. An atomic model of actin filaments cross-linked by fimbrin and its implications for bundle assembly and function. J Cell Biol 2001;153:947–956. [PubMed: 11381081]

Zheng L, Sekerkova G, Vranich K, Tilney LG, Mugnaini E, Bartles JR. The deaf jerker mouse has a mutation in the gene encoding the espin actin-bundling proteins of hair cell stereocilia and lacks espins. Cell 2000;102:377–385. [PubMed: 10975527]

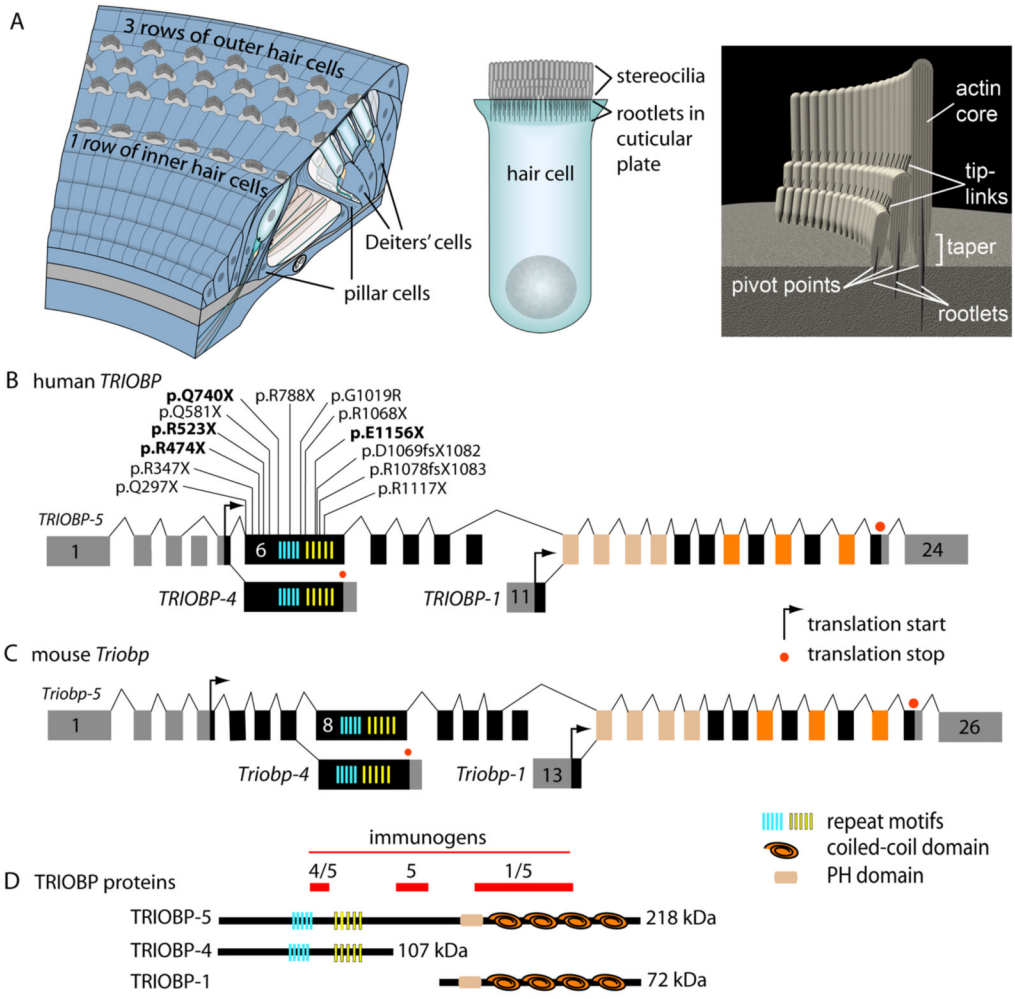

Figure 1. Stereocilia Rootlets within the Organ of Corti and TRIOBP Structure, Isoforms and Immunogens

(A) Organ of Corti schematic showing three rows of outer hair cells (OHCs) and one row of inner hair cells (IHCs) supported by non-sensory pillar cells, Deiter's cells and other supporting cells (left panel). Mechanosensitive stereocilia are arranged into three rows of increasing heights at the apical surface of each hair cell and anchored to the cuticular plate by rootlets protruding into the cell body (middle panel). Unidirectional actin filaments form a paracrystalline core of the stereocilium and become denser at the taper and within the cuticular plate, forming the rootlet (right panel). When stereocilia are deflected, rootlets are bent at the pivot points.

(B) Human *TRIOBP* gene structure showing the three *TRIOBP* transcript classes (TRIOBP-5, TRIOBP-4 and TRIOBP-1), alternative promoters upstream of exons 1 and 11, and thirteen mutations causing DFNB28 deafness that are all located in exon 6 (Riazuddin et al., 2006; Shahin et al., 2006; four novel mutations are shown in bold). *TRIOBP-4* has a translation stop codon and 3' UTR in exon 6. Exon 11 includes the 5' UTR and translation start codon of *TRIOBP-1*. Cassette exons 4 and 10 provide additional variation. Transcripts encoding TRIOBP-1 and TRIOBP-4 share no exons or protein sequence similarity.

(C) Mouse *Triobp* gene structure is similar to human *TRIOBP*. Mouse exon 8 corresponds in sequence to human exon 6.

(D) Three deduced protein isoforms encoded by mouse *Triobp* and predicted domains. Immunogens labeled 4/5, 5 and 1/5 were used to generate antibodies recognizing both TRIOBP-4 and TRIOBP-5, TRIOBP-5 only, and both TRIOBP-1 and TRIOBP-5, respectively.

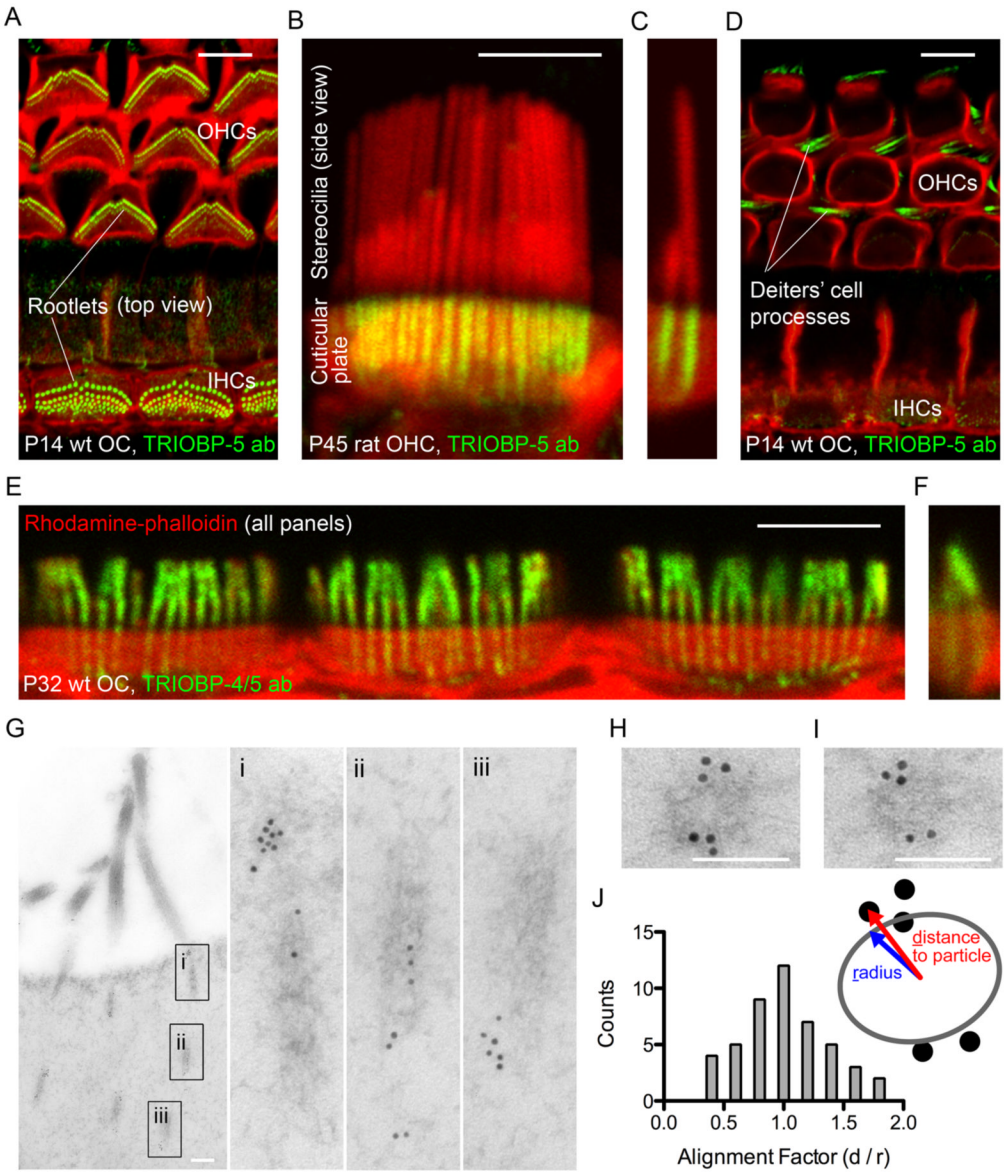

Figure 2. TRIOBP Is Localized to Stereocilia Rootlets

(A) TRIOBP-5 localizes to stereocilia rootlets of wild type (wt) mouse inner (IHCs) and outer (OHCs) hair cells. In all panels A–F, green represents TRIOBP antibody staining (ab), while red is rhodamine-phalloidin staining of the F-actin cytoskeleton. Scale bars in panels A–F, 5 μm.

(B and C) Side view of stereocilia shows rootlets penetrating into the cuticular plate.

(D) TRIOBP-5 labeling in non-sensory Deiters' and pillar cells of the organ of Corti.

(E and F) TRIOBP-4/5 labeling in the rootlets and stereocilia core of IHCs (E) and OHCs (F).

(G) TEM image of post-embedded immunogold labeled transverse sections of stereocilia rootlets in wild type mouse OHCs using TRIOBP-5 antiserum. Insets (i, ii, iii) show magnified views of rootlets. Scale bars, 200 nm.

(H and I) TRIOBP-5 immunogold labeling at the periphery of the stereocilia rootlets in horizontal cross sections. Scale bars, 100 nm.

(J) Gold particles (n = 47, 10 rootlets) are distributed with a modal alignment factor (d/r) close to 1 suggesting predominant localization at the periphery of the rootlet. Age of the specimens: A and D, postnatal day 14 (P14); B and C, P45; E and F, P32; G–I, P6. See also Figure S1.

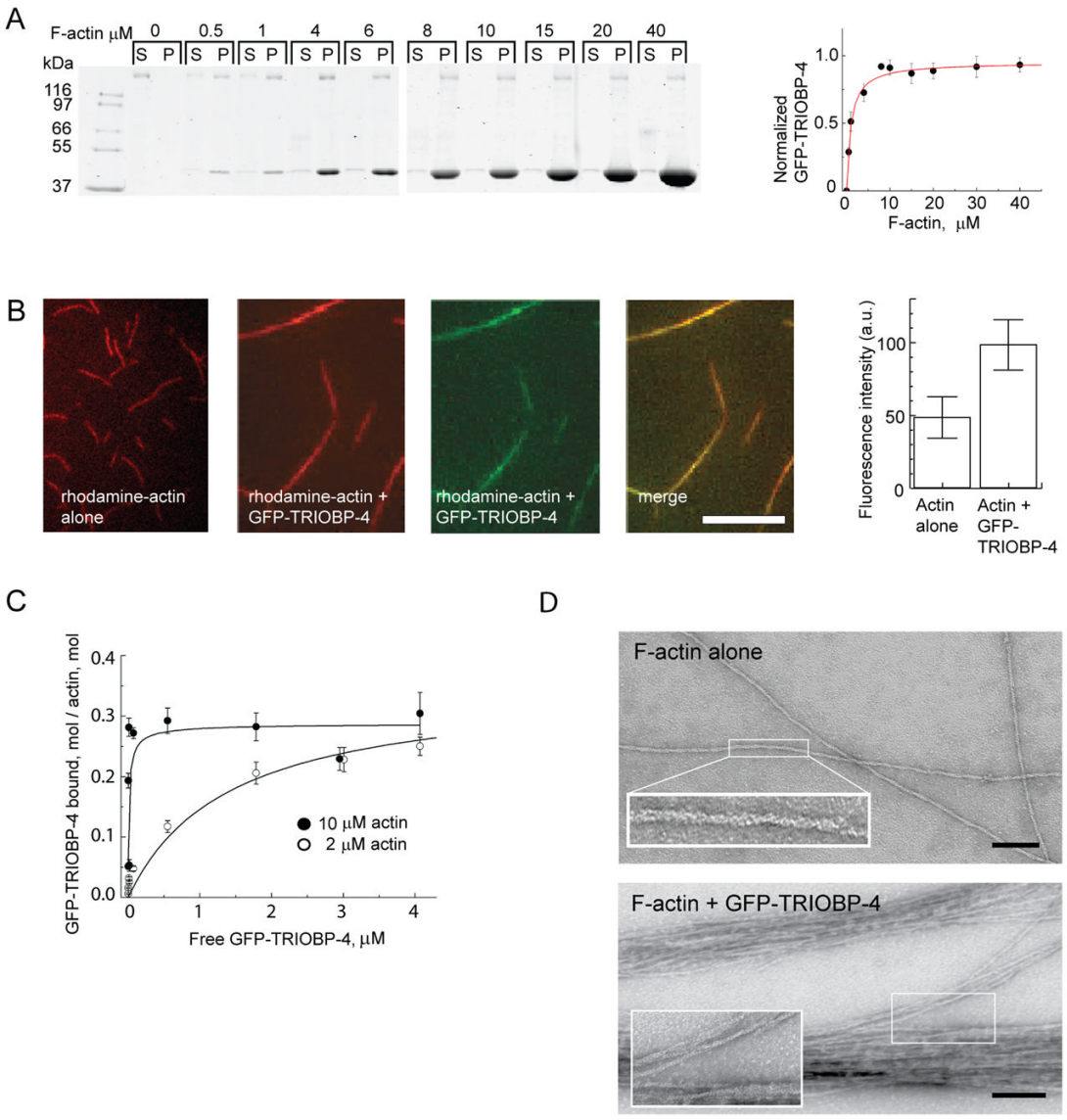

Figure 3. TRIOBP-4 Binds and Bundles Actin Filaments

(A) Binding affinity of GFP-TRIOBP-4 for F-actin measured using high-speed co-sedimentation. Coomassie-stained SDS PAGE analysis (left panel) of 2 μM GFP-TRIOBP-4 mixed with increasing amounts of F-actin (0 to 40 μM, lower band). Supernatants (S) and pellets (P) are shown after 385,000 x g_{max} for 15 min. GFP-TRIOBP-4 (upper band) did not pellet in the absence of F-actin. Bound GFP-TRIOBP-4 was calculated from the amount depleted from supernatants (right panel). The density of each band was measured and normalized to GFP-TRIOBP-4 alone.

(B) GFP-TRIOBP-4 binding to actin (right 3 panels). Left panel shows TIRF imaging of 20% rhodamine-labeled actin filaments without GFP-TRIOBP-4 (red). The next three panels show 20% rhodamine-labeled filaments (red) incubated with 2 μM GFP-TRIOBP-4 (green) and the merge of red and green channels. Scale bar, 10 μm. Right panel shows average fluorescent intensity of rhodamine-labeled F-actin with and without GFP-TRIOBP-4.

(C) Evaluation of the binding of GFP-TRIOBP-4 to F-actin from four independent experiments. The molar ratio of GFP-TRIOBP-4 sedimented at 22,000 x g_{max} for 20 min with

total actin was plotted against free GFP-TRIOBP-4 in the supernatant. Proteins were separated by SDS-PAGE, and the amount of free and bound GFP-TRIOBP-4 quantified using densitometry, plotted and fitted to a hyperbola.
(D) TEM of negative stained 2-D rafts of F-actin alone (left panel) and F-actin bundled with GFP-TRIOBP-4 (right). Insets show the actin filaments at 3X higher magnification. Scale bars, 1 μm.

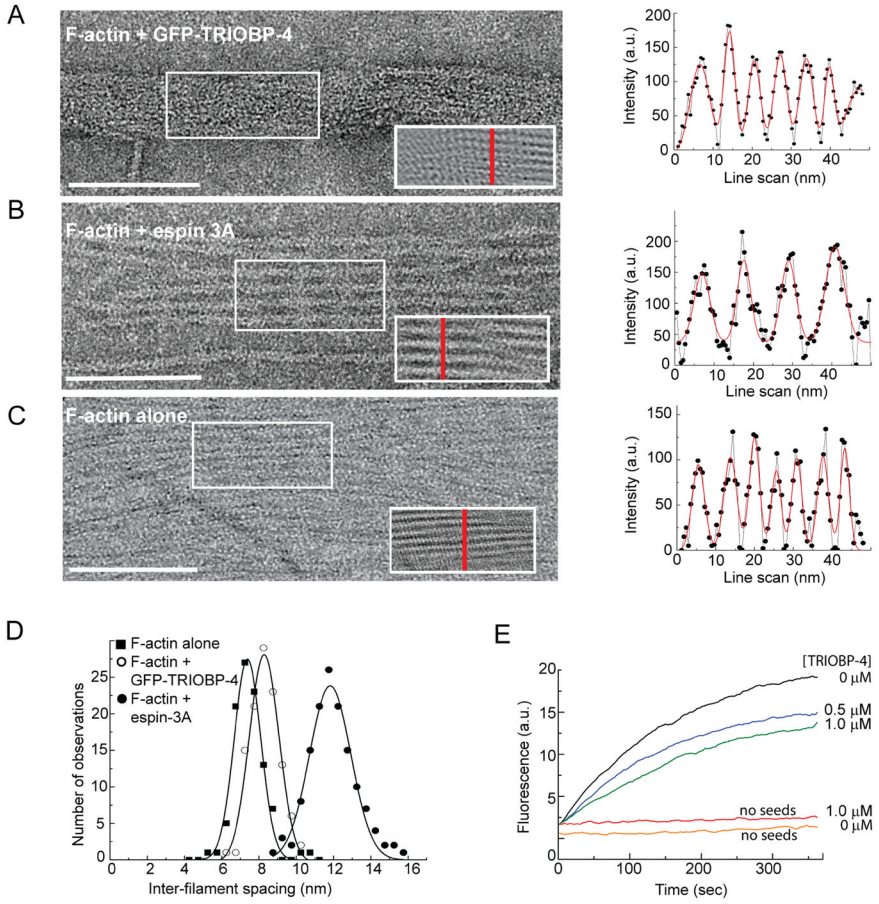

Figure 4. TRIOBP-4 Assembles Actin into the Bundles of Unusually High Density That Resemble Stereocilia Rootlets

(A–C) TEM images of negative stained actin filaments that were formed on a monolayer lipid membrane at a 4:1 molar ratio of actin to GFP-TRIOBP-4 (A), at a 4:1 molar ratio of actin to espin 3A (B), and actin filaments alone at a density that allows stochastic parallel arrangement of filaments (C). Scale bars, 100 nm. Right insets show spatial periodicity of the data within the left inserts that was revealed by FFT filtering. Right panels show the intensity profiles along red vertical scans perpendicular to actin filaments (grey lines, solid circles) and the fit to a sum of Gaussian distributions (red lines).

(D) Histograms of distances between the centers of actin filaments from panels A–C (right) is shown with actin alone (square), actin plus GFP-TRIOBP-4 (open circle) or espin 3A (closed circle). The histograms were fit to a Gaussian distribution.

(E) Purified recombinant TRIOBP-4 inhibits the rate of actin polymerization but does not cause a marked nucleation effect. The plots show solution-based actin polymerization using 10% pyrene-labeled actin (2 μM total actin) with the designated concentration of TRIOBP (μM) in the presence or absence of 0.4 nM actin seeds. Similar results were obtained with GFP-tagged TRIOBP-4. See also Figure S2.

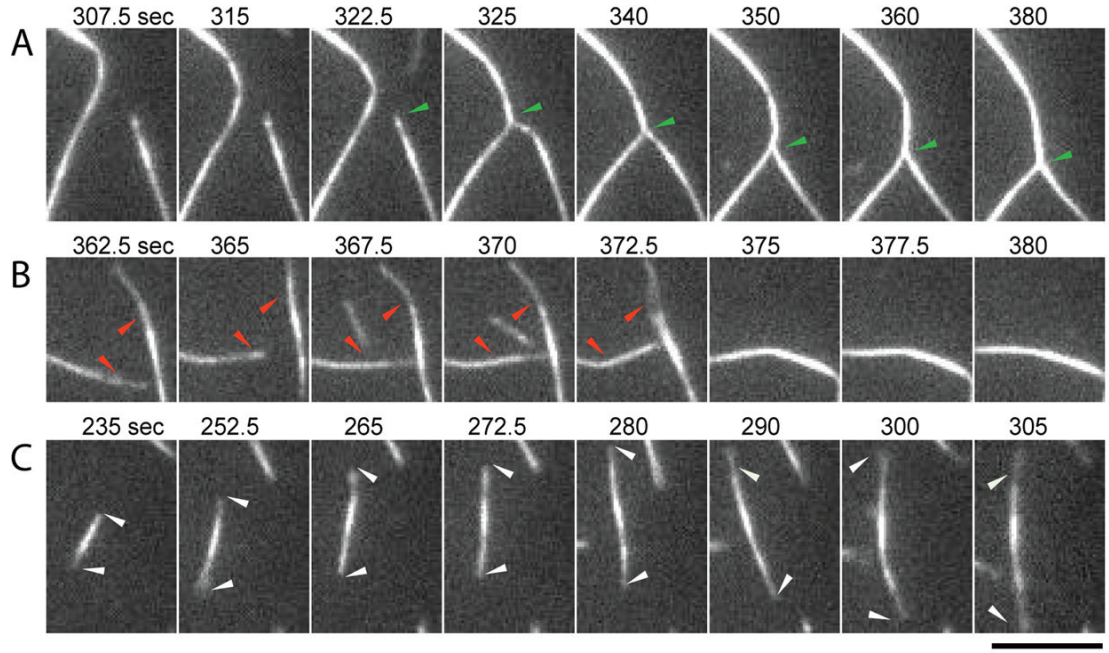

Figure 5. Dynamics of F-actin Bundle Formation with GFP-TRIOBP-4 Observed by Time-lapse TIRF Microscopy

(A) Two F-actin structures coalesce in a zipper-like fashion (green arrows).

(B) Coalescence of F-actin structures that become attached to one another (red arrows).

(C) Bipolar bundles are elongating from both ends (white arrow heads, top row). Scale bar, 5 μm. Movie S1 showing a larger field of view and more examples of bundling behavior is available as supporting information.

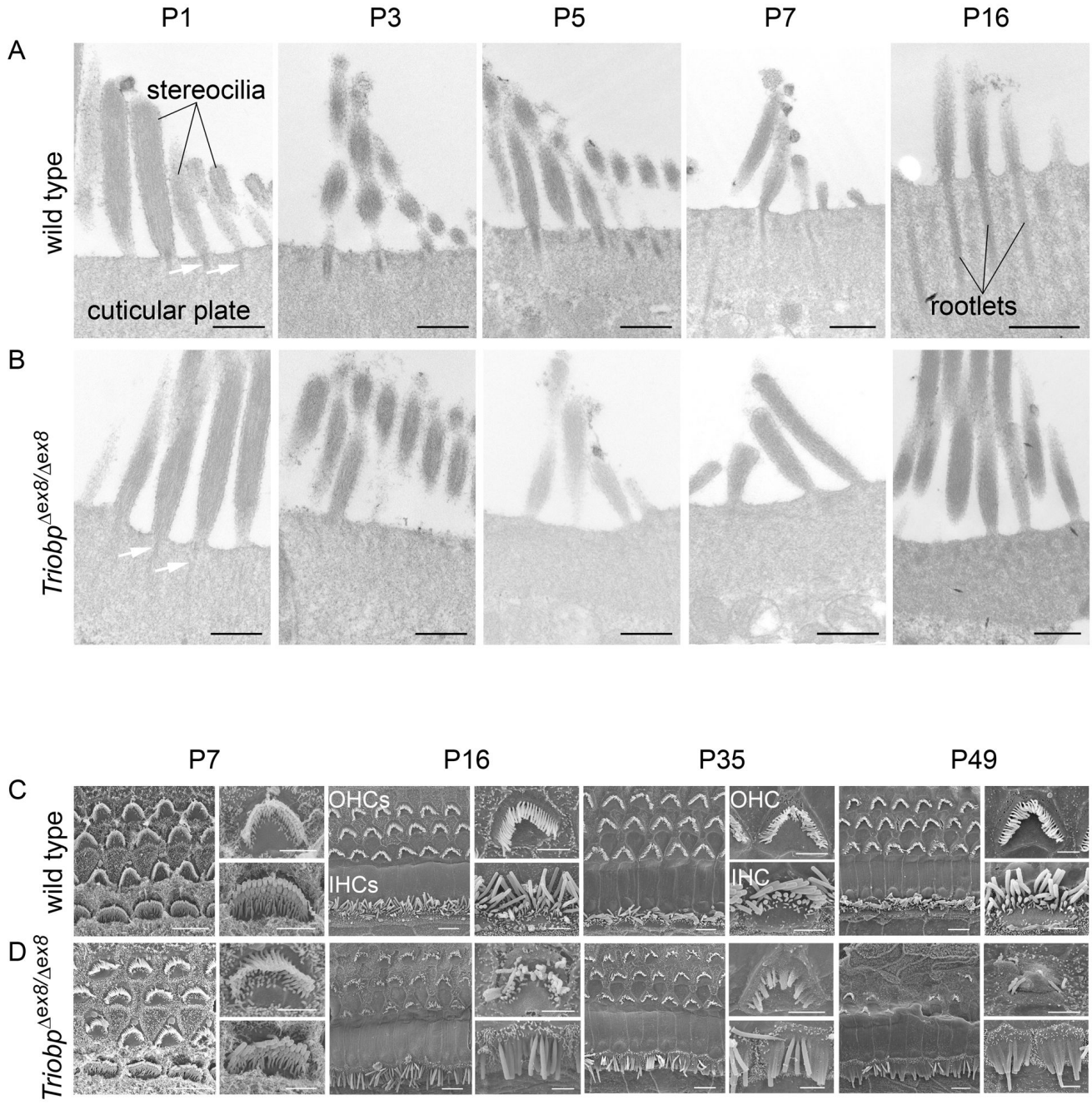

Figure 6. *Triobp*$^{\Delta ex8/\Delta ex8}$ Stereocilia Fail to Develop Rootlets, Fuse Together, and Degenerate

(A and B) TEM images of stereocilia insertions into the cuticular plate in *Triobp*$^{+/+}$ (A) and *Triobp*$^{\Delta ex8/\Delta ex8}$ (B) cochlear hair cells. Scale bars, 500 nm.

(C and D) SEM images of stereocilia bundles of *Triobp*$^{+/+}$ (C) and *Triobp*$^{\Delta ex8/\Delta ex8}$ (D) cochlear hair cells. A set of images is shown for each developmental stage (P7–P49). The left image of each set is a surface view of the organ of Corti showing one row of IHCs (bottom) and three rows of OHCs (upper rows). The upper right image illustrates an OHC at higher magnification, while the right lower image illustrates an IHC. Scale bars, left overview 5 μm; right panels of individual cells, 2 μm. See also Figures S3 and S4.

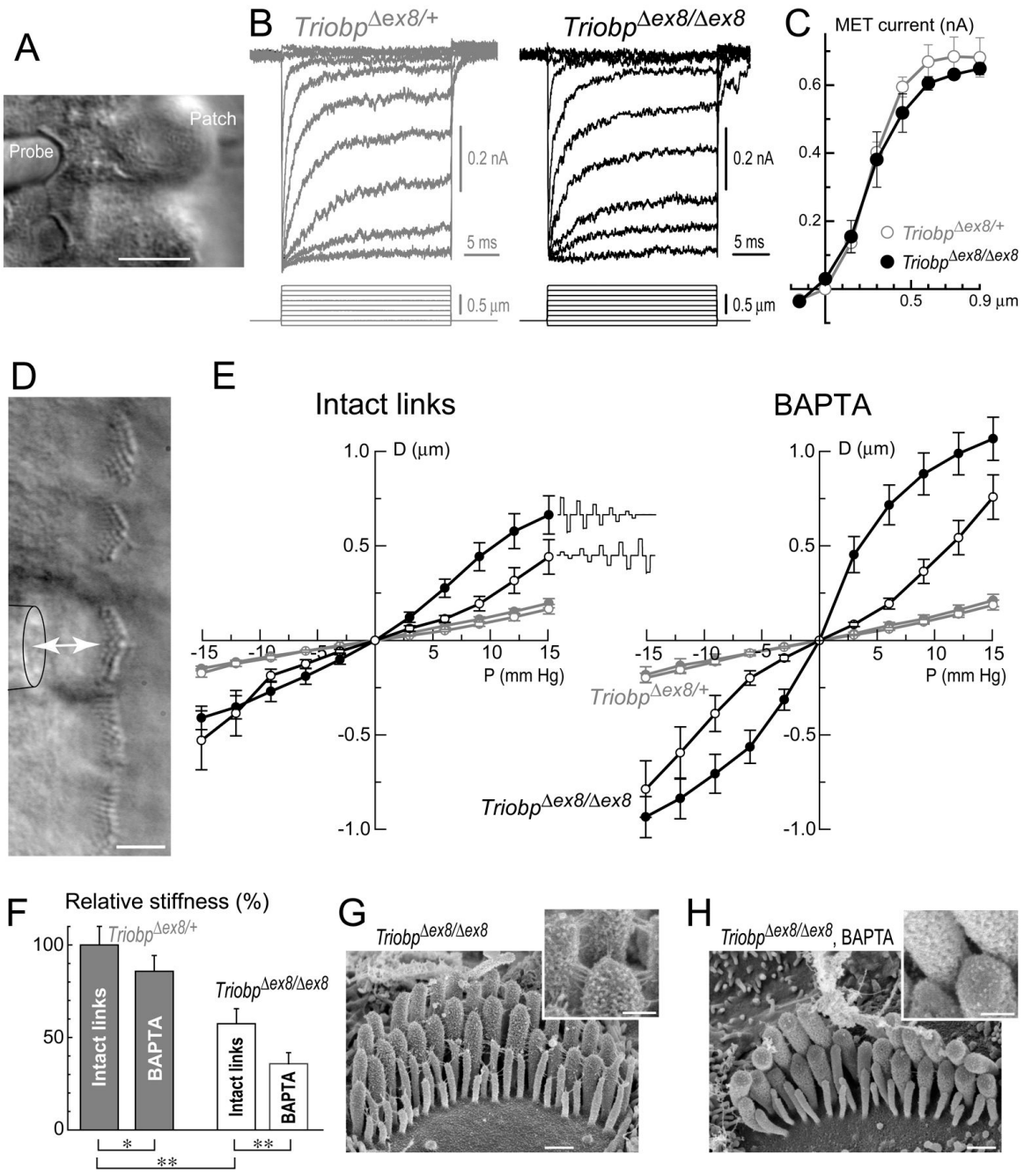

Figure 7. TRIOBP-4/5 Deficiency Does Not Affect Mechano-Electrical Transduction (MET) But Reduces Rigidity of the Stereocilia Bundle

(A) An OHC with a piezo-driven probe (left) and a patch pipette (right). Scale bar, 10 µm.

(B) MET responses (top traces) evoked by graded deflections of stereocilia (bottom traces) in *Triobp*$^{\Delta ex8/+}$ (left) and *Triobp*$^{\Delta ex8/\Delta ex8}$ (right) OHCs. Age of the cells: P2+3 days and P2+2 days *in vitro*, respectively. Holding potential: −80 mV.

(C) Relationship between peak transduction current and probe displacement in *Triobp*$^{\Delta ex8/+}$ (open circles, n=4) and *Triobp*$^{\Delta ex8/\Delta ex8}$ (closed circles, n=3) OHCs. Average data are shown as mean ± SE in all panels.

(D) Deflection of an IHC bundle by fluid-jet. Pressure steps from −15 to +15 mm Hg produced fluid flow (arrow) from the puff pipette (contour on the left) that deflects stereocilia in a positive or negative direction. Scale bar, 5 μm. For quantification of fluid-jet stimuli see Figure S5.
(E) Displacement of tallest stereocilia rank (*D*, μm) as a function of fluid-jet pressure (*P*, mm Hg) in IHCs of *Triobp*$^{\Delta ex8/+}$ (grey symbols) and *Triobp*$^{\Delta ex8/\Delta ex8}$ (black symbols) littermates with intact stereocilia links (left panel) and after application of Ca^{2+}-free solution with BAPTA (right). A single initial large deflection of *Triobp*$^{\Delta ex8/\Delta ex8}$ stereocilia (but not *Triobp*$^{\Delta ex8/+}$) resulted in a very flexible bundle. Thus, stimuli were presented in increasing (open symbols) and decreasing intensity order (solid symbols). Number of cells: *Triobp*$^{\Delta ex8/+}$ (no BAPTA) n = 19 (increasing stimuli), n = 5 (decreasing stimuli); *Triobp*$^{\Delta ex8/+}$ (BAPTA) n = 19 (increasing stimuli), n = 5 (decreasing stimuli); *Triobp*$^{\Delta ex8/\Delta ex8}$ n = 16 (each of four groups). Age of the cells: P4 + 2–4 days *in vitro*.
(F) Relative changes of hair bundle stiffness. Stiffness was assumed to be inversely proportional to the slope (*D*/*P*) of displacement-pressure relationships at low stimuli intensities (from −6 to +6 mm Hg) and expressed as percentage of average stiffness of *Triobp*$^{\Delta ex8/+}$ bundles with intact links. Each bundle was deflected by the same fluid-jet before and after BAPTA application. Stiffness data for *Triobp*$^{\Delta ex8/+}$ IHCs are combined for two different stimuli presentation regimes, as no difference was observed to increasing and decreasing stimuli. Stiffness data for *Triobp*$^{\Delta ex8/\Delta ex8}$ IHCs were collected only for increasing stimuli. Significance was assessed by *t*-test: *Triobp*$^{\Delta ex8/\Delta ex8}$ IHCs vs. control *Triobp*$^{\Delta ex8/+}$ IHCs, independent *t*-test; control vs. BAPTA-treated, paired *t*-test (* - $p<0.05$; ** - $p<0.01$). Number of cells: *Triobp*$^{\Delta ex8/+}$ n = 23; *Triobp*$^{\Delta ex8/\Delta ex8}$ n = 16.
(G and H) SEM images of *Triobp*$^{\Delta ex8/\Delta ex8}$ IHCs incubated in standard HBSS (G) and in Ca^{2+}-free HBSS with 10 mM BAPTA for 5 min (H). Insets show magnified images of stereocilia links. Links between stereocilia were eliminated by BAPTA. Age of the cells: (G) P2+2 days *in vitro*; (H) P3+7 days *in vitro*. Scale bars, 0.5 μm (main panels), 200 nm (insets). See also Figure S5.